IET Nanobiotechnology

Research Article

IET Journals
The Institution of Engineering and Technology

Solvothermal-assisted green synthesis of hybrid Chi-Fe_3O_4 nanocomposites: a potential antibacterial and antibiofilm material

ISSN 1751-8741
Received on 19th February 2020
Revised 9th July 2020
Accepted on 7th August 2020
E-First on 22nd September 2020
doi: 10.1049/iet-nbt.2020.0056
www.ietdl.org

Palanisamy Senthilkumar[1] ✉, Sudhagar Babu[2], Venkatachalam Jaishree[1], Kingsly Joshua Stephen[1], Govindaraj Yaswant[1], Devanesan Sanjeevi Ranjith Santhosh Kumar[3], Nithya S. Nair[3]

[1]*Department of Biotechnology, Kongunadu Arts and Science College, Coimbatore, Tamil Nadu, India*
[2]*Department of Biotechnology, PSG College of Arts and Science, Coimbatore, Tamil Nadu, India*
[3]*School of Biotechnology, Dr. G R Damodaran College of Science, Coimbatore, Tamil Nadu, India*
✉ *E-mail: senthilkumar1185@gmail.com*

Abstract: In this present study, a hybrid Chi-Fe_3O_4 was prepared, characterised and evaluated for its antibacterial and antibiofilm potential against *Staphylococcus aureus* and *Staphylococcus marcescens* bacterial pathogens. Intense peak around 260 nm in the ultraviolet–visible spectrum specify the formation of magnetite nanoparticles. Spherical-shaped particles with less agglomeration and particle size distribution of 3.78–46.40 nm were observed using transmission electron microscopy analysis and strong interaction of chitosan with the surface of magnetite nanoparticles was studied using field emission scanning microscopy (FESEM). X-ray diffraction analysis exhibited the polycrystalline and spinel structure configuration of the nanocomposite. Presence of Fe and O, C and Cl elements were confirmed using energy dispersive X-ray microanalysis. Fourier transform infrared spectroscopic analysis showed the reduction and formation of Chi-Fe_3O_4 nanocomposite. The antibacterial activity by deformation of the bacterial cell walls on treatment with Chi-Fe_3O_4 nanocomposite and its interaction was visualised using FESEM and the antibiofilm activity was determined using antibiofilm assay. In conclusion, this present study shows the green synthesis of Chi-Fe_3O_4 nanocomposite and evaluation of its antibacterial and antibiofilm potential, proving its significance in medical and biological applications

1 Introduction

Magnetite nanoparticles (NPs) have revealed superior impact due to its magnetic property, biocompatibility and size in different areas of biology, medicine and physics [1–3]. The major hindrance in the use of these NPs is their high surface energy and solid dipole–dipole contact between them related with the high surface area to volume ratio, that creates a core uncertainty that leads to the aggregation of the particles [4, 5]. There are several methods to synthesise nanostructured magnetic materials of which co-precipitation method [6], sol–gel method [7], thermal decomposition of organometallic compounds [8], hydrothermal synthesis [9] etc. are used more frequently. [10]. Although some of the physical and chemical methods have shown the synthesis of uniformly sized NPs a major drawback would be lack of stability and high agglomeration of the particles resulting with a different physical property and toxic chemicals used for the synthesis. In contrast, the biological method of NP synthesis using leaf extracts are ecologically feasible and are found extremely stable with very less agglomeration [11–14]. The biological extract used for the synthesis plays a major role in influencing the size of the NPs. In comparison, lower concentration of the extract resulted in an average size <50 nm and higher concentration resulted in an increased size >70 nm [15]. At the same time, the higher concentration of extract also resulted with a smaller size of the NPs [16], these correlates that the amount of phytochemicals, functional groups and metabolites majorly influence the size regardless of the concentration of the extract [17].

On the other hand, the solvothermal method is well known for synthesising rich mesoporous Fe_3O_4 NPs with increased stability due to the use of stabiliser and surfactants [18]. In this study, we adopted to use a solvothermal assisted green synthesis using floral extracts for its efficient biological application. *Talinum portulacifolium*, a medicinal flora of the family *Portulacaceae*, majorly found in the regions of Asia and Africa. The secondary metabolites screening of *T. portulacifolium* leaves extract exhibited the presence of active compounds substantially considered for its anti-diabetic and antioxidant property [19, 20].

Numerous stabiliser and surfactants are being used to increase the stability of Fe_3O_4 NPs, this generates several external modifications on the surface of the particles [21, 22]. Polymers of the biological source are exceedingly preferred as a better solution for stabilising the surface charge of the NPs. A linear polysaccharide of deacetylated beta-1, 4-D-glucosamine, commonly known as Chitosan, a chitin derivative that has been widely used in the area of medicine for its remarkable biological and chemical properties like biodegradability, biocompatibility, hydrogelation, anti-microbial property and polycationic nature [23–28]. Plentiful studies have reported the use of chitosan and magnetic NPs in the form of hybrids, composites etc. that are highly potential and efficient in biological applications. [29–31] Encapsulation of the NP using the polymeric chains of chitosan on holds the stable anionic magnetic core with a cation surface that is functionally improved. Manorjan *et al.* (2015) also showed the modulation of the surface charge potential of iron oxide NP by encapsulation with chitosan. This helps in the improved interaction of the polymer-coated NPs with the surface of the bacteria with relatively high ROS production [28] and its biofilm resulting in better antibacterial activity [32, 33]. Also, recent works show that NPs with an average size of less <50 nm are more effective due to its ability to permeate and disrupt the bacterial cell wall [15, 33].

Nowadays, a major global health concern is the growth and increased tolerance of bacteria against several potential antibiotics [34–36] through the development of bacterial slime and biofilms, thus improving the bacterial resistance [37–39]. The progressing field of nanotechnology and the expansion of various nanomaterials are being considered to address these research problems [40, 41]. The present study shows the development of a magnetite-chitosan nanocomposite by solvothermal assisted green synthesis method and its characterisation using different modern instrumentation. To the best of our knowledge, this is the first report on the solvothermal assisted green synthesis of hybrid

chitosan-magnetite nanocomposite using *T. portulacifolium* leaf extract. The main objective of the study is to develop a stable surface charge modified magnetite-chitosan nanocomposite and evaluation of its enhanced properties, surface interactions and its biological applications.

2 Materials and methods

2.1 Chemicals

Iron (II) chloride tetrahydrate ($FeCl_2{\cdot}4H_2O$), iron (III) chloride hexahydrate ($FeCl_3{\cdot}6H_2O$), ethylene glycol and chitosan ($C_{56}H_{103}N_9O_{39}$) (low-molecular weight, degree of deacetylation 70–90%), were procured from HiMedia, India. All the reagents were prepared using deionised water from Merck Millipore Laboratory water purification system, Germany. The clinical isolated Gram-negative bacteria *Staphylococcus marcescens* and *Staphylococcus aureus* were obtained from the Aravind eye hospital, Coimbatore, Tamilnadu, India.

2.2 Microbial cultures

The procured bacterial strains *S. marcescens* and *S. aureus* were serial diluted and were swabbed on an agar plates of Mueller Hinton agar (MHA) medium to acquire the desired colony forming units (CFUs) (1.5×10^8 CFU/mL).

2.3 Synthesis of Fe_3O_4 NPs

The plant extract is prepared by boiling 5 g of (dried and powdered) leaf in 100 mL distilled water 80°C for 30 min. $FeCl_2{\cdot}4H_2O$ and $FeCl_3{\cdot}6H_2O$ solution was prepared at the ratio of 1:2 M and mixed with 100 mL of plant extract, to which 60 mL of ethylene glycol solution was added. The resulting solution was kept at 80°C for 10 min under continuous stirring on a magnetic stirrer, during which the solution was observed for the development of yellowish colour. To this solution, 10 mL of 1.0 M freshly prepared NaOH solution was added dropwise at a rate of 3 mL/min, permitting constant magnetite precipitation under continuous stirring and the mixture was adjusted to pH 11.

A colour change from yellow solution to a black coloured solution was observed after 30 min, after which the solution was placed in a Teflon-lined stainless-steel autoclave and was maintained at a temperature of 160°C for 12 h. The solution was thawed to the room temperature gradually. The prepared Fe_3O_4 NPs (magnetite NPs) were collected using continuous centrifugation and washed with deionised water to remove all the remains of leaf extract. The concentrated NPs were dried in an oven at a temperature 80°C for 24 h and stored in an air-tight container for further analysis.

2.4 Preparation of hybrid Chi-Fe_3O_4 nanocomposite

About 200 mg of the synthesised Fe_3O_4 NPs were added to 20 mL of chitosan solution (20 mg of chitosan in 20 mL of 1% acetic acid) under continuous stirring at room temperature for 2 h. The obtained hybrid chitosan-magnetite nanocomposites (Chi-Fe_3O_4) were washed with double distilled water and concentrated by centrifugation at 5000 rpm for 15 min. The NPs were calcinated at 40°C for 1 h to remove excess chitosan and dried in an oven at 60°C for 24 h.

2.5 Characterisation techniques

The techniques used for the characterisation of hybrid Chi-Fe_3O_4 nanocomposite are as follows: The formation of hybrid Chi-Fe_3O_4 nanocomposite was primarily confirmed using ultraviolet–visible (UV-Vis) spectroscopy (JASCO-V-670), the spectrum recorded a strong peak at the range of 200–600 nm at a resolution of 1 nm. The transmission electron microscopy (TEM, Technai G2, at 200 kV) was used for analysing the morphology and size of the hybrid Chi-Fe_3O_4 nanocomposite. The crystalline nature of hybrid Chi-Fe_3O_4 nanocomposite was confirmed using a Rigaku Miniflex diffractometer with Cu-Kα radiation and the X-ray diffraction (XRD) diffraction pattern was analysed at the range of 20°–80°. The surface morphology of the hybrid Chi-Fe_3O_4 nanocomposite was studied using field emission scanning microscopy (HITACHI SU6000 FESEM). Energy-dispersive X-ray microanalysis (EDS, R Model Quan Tax 200, Germany) was used to analyse the chemical composition of the hybrid Chi-Fe_3O_4 nanocomposite. The functional group examination of hybrid Chi-Fe_3O_4 nanocomposite was analysed by Fourier transform infrared (FTIR) spectroscopic analysis (Shimadzu IR-Prestige-21), read at the range of 400–4000 cm^{-1}. The zeta potential was studied with Zeta sizer-NanoZs (Malvern Instruments) at 25°C to understand the surface charge of hybrid Chi-Fe_3O_4 nanocomposite. Dynamic light scattering (DLS) spectroscopy was used for calculating the average size of hybrid Chi-Fe_3O_4 nanocomposite, by dispersing hybrid Chi-Fe_3O_4 nanocomposite samples in de-ionised water.

2.6 Minimum inhibitory concentration (MIC) determination

The MIC of hybrid Chi-Fe_3O_4 nanocomposite against *S. marcescens* and *S. aureus* was studied using the protocols reported by CLSI-Clinical and Laboratory Standards Institute [42]. The bacterial pathogens were cultured in Mueller–Hinton broth (MHB) at 37°C overnight and diluted to produce 5×10^5 CFU/mL. Sterile culture media of 200 µL was used as control. Chi-Fe_3O_4 nanocomposite of different concentrations (0.5, 1, 10, 25, 50, 75, 100 µg/mL) was introduced to 200 µL of overnight grown cultures taken in a polypropylene 96-well microplate and was incubated at 37°C for 24 h. The absorbance was noted before and after incubation at 550 nm. In the intervening time, the minimum bactericidal concentration (MBC) was also determined using the lowest concentrations.

2.6.1 Antibacterial activity determination: The hybrid Chi-Fe_3O_4 nanocomposite was studied for its antibacterial activity against *S. marcescens* and *S. aureus* using standard agar well diffusion method. Briefly, the pathogenic bacterial strains *S. marcescens* and *S. aureus* (1.5×10^8 CFU/mL) were swabbed on agar plates containing Muller–Hinton medium. Hybrid Chi-Fe_3O_4 nanocomposite was dispersed in sterile distilled water at the concentration of 1 mg/1 mL. Wells of 5 mm in diameter were made on agar plates using a well puncher and were loaded with different concentrations of 10, 25, 50 and 100 µL of hybrid Chi-Fe_3O_4 nanocomposites. The antimicrobial activity was determined by measuring the zone of inhibition around the wells of the agar plates incubated for 24 h at 37°C.

In addition, the surface morphology of the bacterial cells was observed using light microscopy and FESEM. Overnight grown *S. marcescens* and *S. aureus* cultures of 200 µL were incubated with 100 µL of hybrid Chi-Fe_3O_4 nanocomposite (1 mg/1 mL sterile water) for 3 h, where the untreated cultures served as control. The bacterial cells were collected by centrifugation after the incubation, washed twice with 0.85% NaCl, and fixed on to a glass slide with 2% glutaraldehyde at room temperature (~25°C). The fixed cells were resuspended in double-distilled water and dehydrated on silicon substrate chips.

2.6.2 Congo red agar assay: The formation of bacterial biofilms was confirmed using Congo red agar method [43]. The overnight bacterial cultures of *S. marcescens* and *S. aureus* were inoculated on brain heart infusion agar plate containing 5% sucrose supplement and 0.8 µg of Congo red and incubated for 24 h at 37°C. Black-coloured colonies indicate the positive formation of biofilm with a dry crystalline consistency.

2.6.3 Antibiofilm assay: The antibiofilm activity of hybrid Chi-Fe_3O_4 nanocomposite was done by using the method of Nithya *et al.* [44]. The bacterial pathogenic *S. marcescens* and *S. aureus* biofilms were grown in LB medium supplemented with 5% sucrose in a 24-well polystyrene plate at 30°C for 24 h. After the incubation, the contents in the wells were discarded and the plates

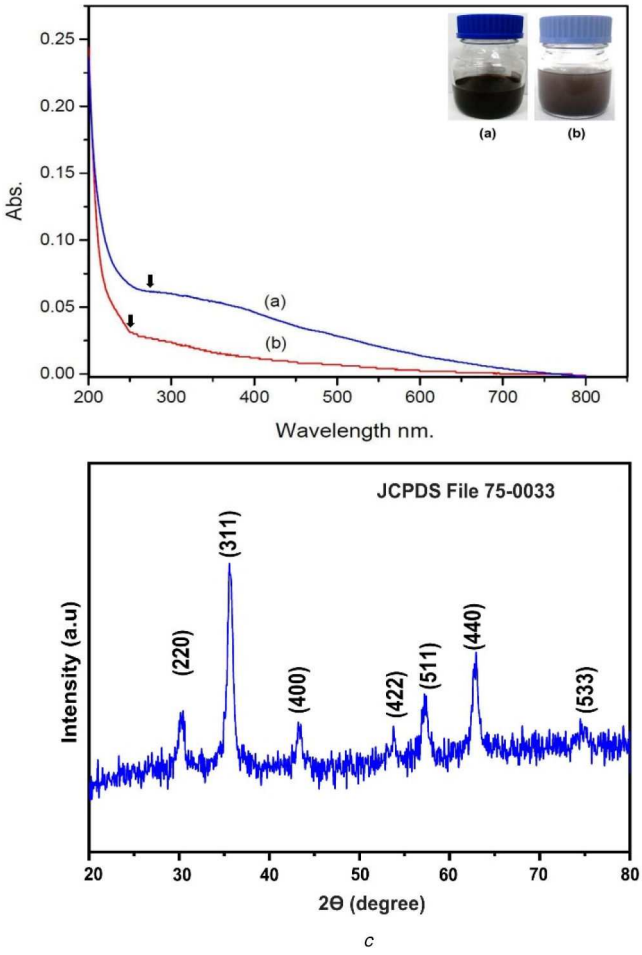

Fig. 1 *UV-Vis spectrum of Chi-Fe_3O_4 nanocomposites*
(a) Fe_3O_4 NPs, ***(b)*** Chi-Fe_3O_4 nanocomposites, ***(c)*** XRD analysis of Chi-Fe_3O_4 nanocomposites

were washed with phosphate-buffered saline twice. Further, they were washed with distilled water for the removal of the remaining non-adhered cells. The adhered immobile cells with biofilms were stained with 0.4% (w/v) crystal violet stain for 5 min and were washed with distilled water. Different concentrations of hybrid Chi-Fe_3O_4 nanocomposite (ranging from 5 to 50 µg/mL) were added to the wells, where untreated well with cells and biofilm served as the control. The plates were incubated for 24 h at 37°C. In total, 1 mL of absolute ethanol was pipetted to each well to dissolve the crystal violet staining the cells and biofilms. The absorbance was noted at 570 nm and the percentage of biofilm inhibition was calculated using the following formula:

$$\text{Percentage of inhibition } (\%) = \left[\frac{\text{control OD} - \text{test OD}}{\text{control OD}}\right] \times 100 \quad (1)$$

2.6.4 Statistical analysis: All the experiments were done in triplicates, and the results were presented as mean ± standard deviation ($n = 4$). The experimental data were analysed using Statistical Package for the Social Sciences (SPSS) (SPSS version 14. IBM Corporation). $P < 0.05$ was considered as statistically significant.

3 Results and discussions

3.1 Preparation of Chi-Fe_3O_4 nanocomposite

The development of Fe_3O_4 NPs (magnetite NPs) was preliminarily confirmed by the colour change from pale yellow to black colour when kept in a Teflon-lined stainless-steel autoclave (see Fig. 1*a*). In discussion with the results reported by Kouhbanani *et al.*, [45] the synthesised Fe_3O_4 NPs formed a black colour solution. The occurrence of various phytocompounds from *T. portulacifolium* leaf extract that gives the ability to reduce $FeCl_2$ and $FeCl_3$ to $Fe_{3}o_4$ NPs

Buazar *et al.* [46] studied the mechanism of Fe_3O_4-NPs formation using a potato. He showed that extract plays an important role in reducing agents and as capping in the Fe_3O_4-NPs formation. The reaction started in addition of NaOH and produced the oxidation of starch in alkaline solution these oxidations produced electrons that reduced Fe^+ ions to Fe^0 NPs. In the interim, the starch primary hydroxyl groups were oxidised to the carboxyl group. He also showed that the problem of aggregation of NPs in water was overcome as Fe_3O_4-NPs dissolved in potato extract easily.

After the addition of chitosan solution with the synthesised Fe_3O_4 NPs, a change in colour from black suspension to brown was noted directly in the reaction mixture (see Fig. 1*b*). The change of brown colour indicates the formation of Chi-Fe_3O_4 nanocomposite. These results are supported by the work of Nehra *et al.*, [47] who observed similar colour change during the preparation of chitosan-coated magnetic NPs. The hydroxyl and amine groups of the chitosan is a suitable capping agent for the synthesis of metal NPs and the presence of amine group in chitosan has a strong affinity towards metal ions hence it helps the binding of chitosan to the metal [48].

3.2 Characterisation techniques

3.2.1 UV-Vis spectroscopy: The UV-Vis spectrum of both Fe_3O_4 NPs and the hybrid Chi-Fe_3O_4 nanocomposite were measured at 200–800 nm range. The absorbance peak characteristic to Fe_3O_4 NPs was obtained at 260 nm (see Fig. 1*a*). The previous report

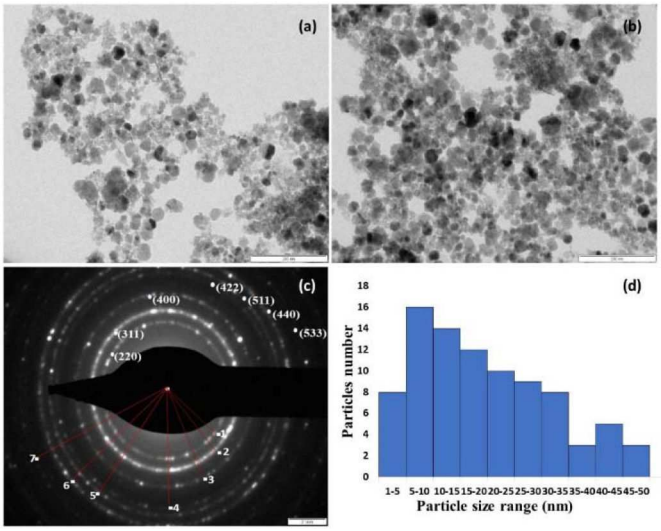

Fig. 2 *TEM analysis of Chi-Fe_3O_4 nanocomposites*

(a), ***(b)*** TEM images of hybrid Chi-Fe3O4, ***(c)*** SAED pattern, ***(d)*** Particle size distribution

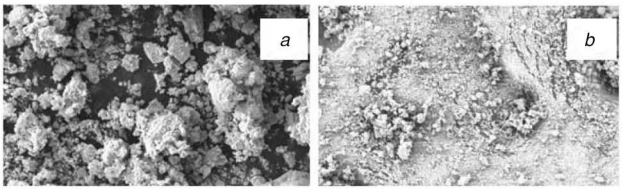

Fig. 3 *FESEM analysis of Chi-Fe_3O_4 nanocomposites*

(a) FESEM image at 3.14 kx magnification, ***(b)*** FESEM image at 408 X magnification

states the spectral absorbance around 260 nm is a characteristic feature of Fe_3O_4 NPs [49]. After the adding of chitosan solution into the synthesised Fe_3O_4 NPs, the change in absorbance shift was noticed at 272 nm and the broadening absorbance spectral alterations initially support the surface modifications of FeO NPs [50].

3.2.2 XRD analysis: XRD pattern of the hybrid Chi-Fe_3O_4 nanocomposite is shown in Fig. 1*c*. Major diffraction peaks 311, 220, 400, 422, 511 and 440 were noted at the planes 35°, 30°,43°, 53°, 57° and 62°, respectively. This confirms that the magnetite-Fe_3O_4 NPs possess a spinel structure with polycrystalline nature. The 2θ value of the diffraction peak 311 was considered as the confirmation for Fe_3O_4 NPs. As reported in various previous literature works, the standard diffraction peak 311 at 35.423° corresponds to for magnetite formation [51]. The obtained XRD analysis data of hybrid Chi-Fe_3O_4 nanocomposite was reliable with standard JCPDS reference code–75-0033 [15, 28]. The crystallite size of the hybrid Chi-Fe_3O_4 nanocomposite was calculated by the Scherrer ((2)) [52]

$$D = \frac{K\lambda}{\beta \cos\theta} \tag{2}$$

where D = average crystallite size, K-shape constant, λ – wavelength of X-ray, β – full width half maximum (FWHM) of refection (in radians) located at 2θ and θ – angle of reflection (in degrees). The crystalline size of the composite was determined to be 7.13 nm, derived from the FWHM of the corresponding peak at 311.

3.2.3 TEM analysis: TEM images of hybrid Chi-Fe_3O_4 nanocomposite were shown in Figs. 2*a* and *b*. The obtained TEM results of hybrid Chi-Fe_3O_4 nanocomposite reveals that most of the particles are spherical in shape with less agglomeration. These also show the polycrystalline nature of the composite with a particle size distribution of 3.78–46.40 nm (see Fig. 2*d*). Similar findings were reported by Pati *et al.* [53] who have synthesised spherical-shaped Chitosan-functionalised Fe_3O_4 at Au nanomaterials with different size range from 10 to 40 nm.

3.2.4 FE-SEM and EDS analysis: Surface morphology and elemental composition the of hybrid Chi-Fe_3O_4 nanocomposite was determined by FESEM and energy dispersive spectroscopy, respectively, shown in Figs. 3*a* and *b*. The images attained using FE-SEM shows the predominantly spherical-shaped particles with high aggregation, this may be due to the strong inter-particle's Van der Waals force and magnetic attraction among the Fe_3O_4NPs [54]. The chitosan was strongly bound on the surface of the hybrid Chi-Fe_3O_4 nanocomposite. Similar observations were noticed in the previous report by Unsoy *et al.* [55].

In addition, the EDS spectrum of the nanocomposite exhibited the presence of Fe and O, C and Cl (see Fig. 4*b*). This clearly states the formation of Fe_3O_4 and the absence of any other peaks indicating the purity of hybrid Chi-Fe_3O_4 nanocomposite. The presence of Fe, O and C in the EDS spectrum of chitosan-coated nanomaterials supports the precursor material in the synthesis of hybrid Chi-Fe_3O_4 nanocomposite. The weak carbon (C) signals produced may be due to the presence of chitosan that encapsulates the Fe_3O_4 [56, 57]. The detection of C in the EDS spectrum also supports the presence of chitosan polymer in the prepared nanocomposite. Similar findings were reported by Manikantan *et al.*, [52] who have documented the presence of C in the prepared copper-chitosan NPs. The functional groups Cl and O signals in the EDS spectrum corresponds to the X-ray emission from proteins bound to the NPs surface, which were then removed by centrifugation followed by repeated washing of the composite [58].

3.2.5 FTIR analysis: The FTIR spectrum of hybrid Chi-Fe_3O_4 (see Fig. 5) showed sharp peaks (cm^{-1}) 3502.73, 3329.14, 2303.03, 1743.65, 1643.35, 1519.91, 1369.46 and 1215.15 corresponds to O–H stretching vibrations, hydroxy group (H-bonded OH stretch), N–H stretching (for chitosan), alkyl carbonate, carbonyl groups, aromatic nitro compounds, carboxylate (carboxylic acid salt) stretching and C–C aromatic ring/C–OH stretching vibrations, respectively, attributing to the functional groups from the reduction of NPs. The peaks 636.51 attributes to the iron oxide skeleton, the peaks 597.93, 540.07, 501.49 are characteristic to Fe_3O_4NPs corresponding to the aliphatic Iodo compounds, C–I stretch. In addition 466.77 indicated aryl disulphides (S–S stretch) attribute the intrinsic stretching vibrations of the Fe at a tetrahedral site. In discussion with the works of Nasrollahzadeh *et al.* (2016) [59] and Sathishkumar *et al.* [60] similar characteristic peaks were found at the range of 500–600 with the iron oxide skeleton. Zulfikar *et al.* [61] and Tiwari *et al.* [62] also showed a similar range of peaks

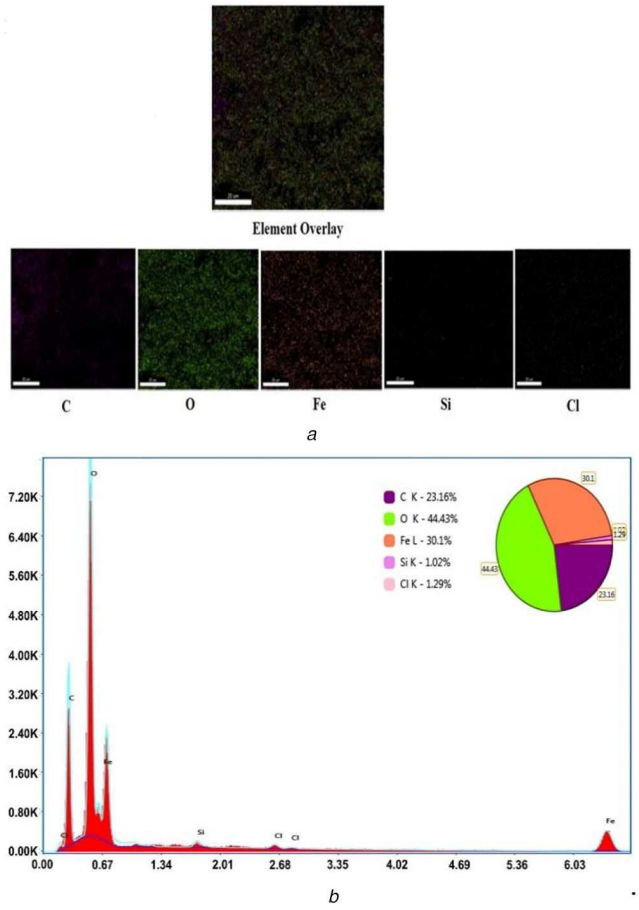

Fig. 4 *EDS analysis and elemental mapping*
(a) Elemental mapping, ***(b)*** EDS analysis of Chi-Fe_3O_4 nanocomposites

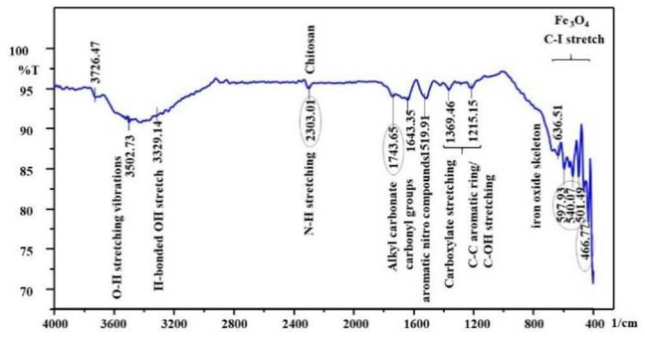

Fig. 5 *FTIR analysis of Chi-Fe_3O_4 nanocomposites*

that are characteristic to Fe_3O_4 and Chitosan. The increased intensities of N–H vibrations for hybrid Chi-Fe_3O_4 nanocomposite determine the surface coating of chitosan on negatively charged Fe_3O_4NPs, which indicates a strong interaction between the amino group on chitosan molecules and Fe_3O_4NPs.

3.2.6 Zeta potential analysis and DLS studies: The zeta potential measurements for synthesised hybrid Chi-Fe_3O_4 nanocomposite were presented in Figs. 6*a* and *b*). The Zeta potential value of −78.9 mV shows that the surface of the hybrid Chi-Fe_3O_4 nanocomposite is negatively charged, and this constitute interaction of the particles with each other and consequently contributing to a stable particle size of the sample. Our results were similar to the previous report by Banerji *et al.* [63]. The DLS studies showed the *Z* average size diameter of 1288.0 nm for hybrid Chi-Fe_3O_4 nanocomposite (see Fig. 6*c*). The results of DLS analysis shows the increased size of the nanocomposite in comparison to TEM results, this is because DLS measures the hydrodynamic size of the synthesised NPs [64, 65].

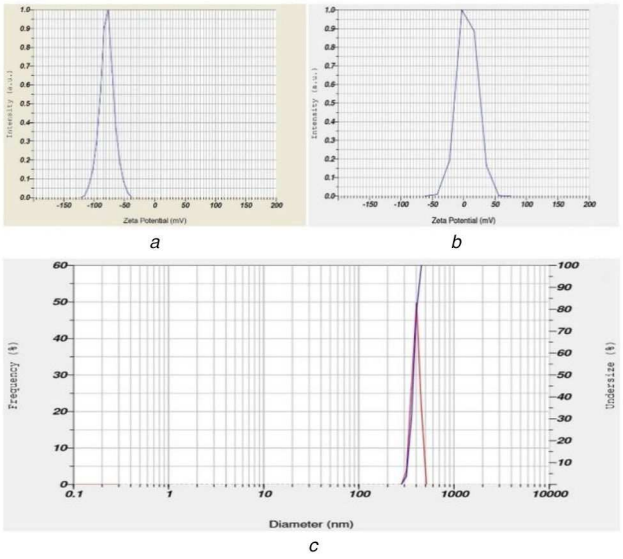

Fig. 6 *Zeta potential and DLS analysis*
(a) Zeta potential analysis of Fe_3O_4, ***(b)*** Zeta potential analysis of Chi-Fe_3O_4 nanocomposites, ***(c)*** DLS studies of Chi-Fe_3O_4 nanocomposites

Table 1 MIC and MBC Chi-Fe_3O_4 nanocomposites against tested organisms

Bacterial samples	MIC, µg/mL	MBC, µg/mL
S. marcescens	47	45
S. aureus	39	36

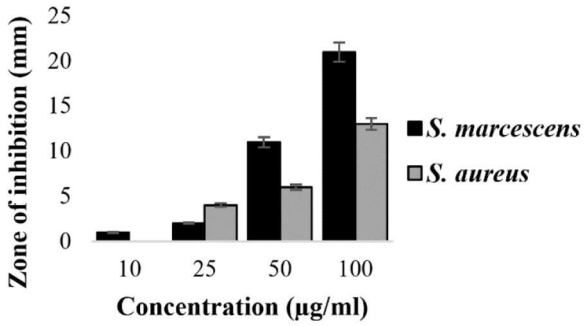

Fig. 7 *Antibacterial activity of Chi-Fe_3O_4 nanocomposites against S. marcescens, S. aureus*

3.3 MIC and MBC determination

MIC and MBC of hybrid Chi-Fe_3O_4 nanocomposite against *S. marcescens* and *S. aureus* were determined to be 47 and 39 µg/mL, respectively (see Table 1). The MIC and MBC results showed the hybrid Chi-Fe_3O_4 nanocomposite were effective against both *Escherichia. coli* and *S. aureus*, making it a good nanomaterial for the treatment against pathogenic bacteria.

3.4 Antibacterial activity

On evaluating the antibacterial activity of the nanocomposite against the bacterial strains using standard agar well diffusion method, strong antibacterial activity was observed against *S. marcescens* at 21 mm at the concentration of 100 µL, followed by *S. aureus* at 13 mm at the concentration of 100 µL. Whereas 10 and 25, 50 µL concentration showed moderate activity of 1, 2 and 11 mm, respectively, against *S. marcescens* and 0, 4 and 6 mm, respectively, against *S. aureus* (see Fig. 7).

Furthermore, the morphological changes of hybrid Chi-Fe_3O_4 nanocomposite treated and untreated *S. marcescens* and *S. aureus* cultures were observed using light microscopy and FESEM analysis (see Fig. 8). At the highest concentration of 100 µL of hybrid Chi-Fe_3O_4 nanocomposite treated against both test,

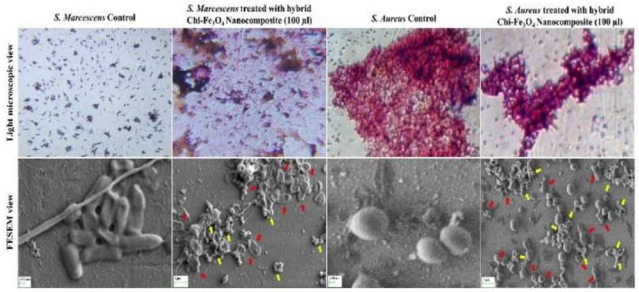

Fig. 8 *FESEM and Light microscopic view of Chi-Fe_3O_4 nanocomposites treated and control pathogens of S. aureus and S. marcescens*

Fig. 9 *Congo red method of biofilm confirmation*
(a) *S. marcescens*, ***(b)*** *S. aureus*

organisms exhibited significant morphological changes of cell membranes, where no morphological changes were observed in the untreated bacterial cultures. The morphological changes on the bacterial membrane surface on treatment with hybrid Chi-Fe_3O_4 nanocomposite (Scheme 1), indicates its ability to break and penetrate the cell membrane. It is also considered that the composite can also damage the DNA and denatured the cellular proteins [66, 67].

3.5 Congo red method

The Congo red agar method confirmed the formation of biofilms after 48 h indicated by the growth of black colour colonies. 92.20 and 87.32% of the colonies respective to *S. marcescens* (see Fig. 9*a*) and *S. aureus* (see Fig. 9*b*) grown was observed to be black in colour with dry crystalline consistency.

3.6 Antibiofilm activity

The antibiofilm activity of hybrid Chi-Fe_3O_4 nanocomposite against *S. marcescens* and *S. aureus* pathogens was done using the crystal violet assay. After the 24 h of treatment, nanocomposite at the concentration of 5–50 µg/mL resulted in greater inhibition of 72.8–85.5% (see Figs. 10*a* and *b*).

On treating *S. marcescens* and *S. aureus* using 5 µg/mL hybrid Chi-Fe_3O_4 nanocomposite significant inhibition of 41.4 and 50.2% was observed, respectively, where 13.7 and 16.4% of inhibition, respectively, was observed when the nanocomposite concentration increased to 20 µg/mL. At a concentration of 50 µg/mL nanocomposite treatment on the pathogens for 24 h, only 10 and 11% bacterial colonies were observed. Hence it is reasonable that the biofilm inhibition activity of hybrid Chi-Fe_3O_4 nanocomposite directly proportional to the concentration used (see Fig. 10). The previous reports also showed similar activity on the increase of the respective materials [68].

4 Conclusion

In conclusion, experimental results showed that the hybrid Chi-Fe_3O_4 nanocomposite prepared using solvothermal-assisted green synthesis method possesses significant physical and chemical properties, with potential antibacterial and antibiofilm nature. Thereby, opening doors for the use of this hybrid Chi-Fe_3O_4 nanocomposite for several biological and medical applications like antimicrobial formulations, packaging of food materials, water treatment and so on. In future, hybrid Chi-Fe_3O_4 nanocomposite can be considered as a substantial material to treat rapidly increasing antibiotic-resistant pathogens.

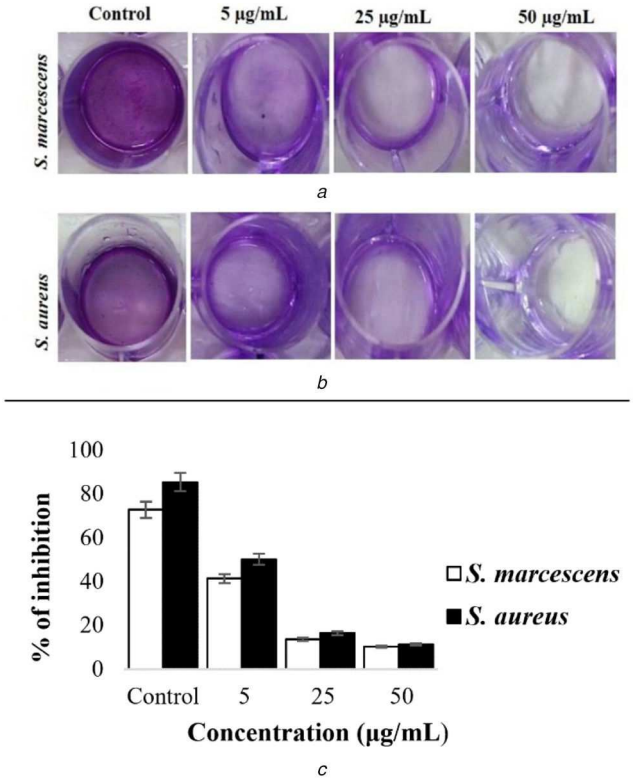

Fig. 10 *Antibiofilm activity of Chi-Fe_3O_4 nanocomposites against*
(a) *S. marcescens*, ***(b)*** *S. aureus*, ***(c)*** % of inhibition of biofilm formation by Chi-Fe_3O_4 nanocomposites

5 Acknowledgments

The authors would like to thank Department of Science and Technology (DST-FIST), India for the grants provided (Grant No. DST-FIST/120/2012) to establish laboratory facilities at Department of Biotechnology Kongunadu Arts and Science College, Coimbatore, Tamilnadu, India. The authors gratefully acknowledge CNR RAO Research centre, Avinasilingam Institute for Home science and Higher Education for Women for the XRD, EDS, FESEM and FTIR analysis. We also extend our thanks to SAIF, IIT Bombay, India for the TEM analysis. P.S., S.B., V.J., K.J., G.Y., D.S.R.S.K. contributed equally to this work.

6 References

[1] Revia, R.A., Zhang, M.: 'Magnetite nanoparticles for cancer diagnosis, treatment and treatment monitoring: recent advances', *Mater. Today*, 2016, **19**, pp. 157–168
[2] Ling, D., Lee, N., Hyeon, T.: 'Chemical synthesis and assembly of uniformly sized iron oxide nanoparticles for medical applications', *Acc. Chem. Res.*, 2015, **48**, pp. 1276–1285
[3] Seabra, A.B., Haddad, P., Duran, N.: 'Biogenic synthesis of nanostructured iron compounds: applications and perspectives', *IET Nanobiotechnol.*, 2013, **7**, (3), pp. 90–99
[4] Pérez, N., Moya, C., Tartaj, P., *et al.*: 'Aggregation state and magnetic properties of magnetite nanoparticles controlled by an optimized silica coating', *J. Appl. Phys.*, 2017, **121**, p. 044304
[5] Gavilán, H., Posth, H., Bogart, O., *et al.*: 'How shape and internal structure affect the magnetic properties of anisometric magnetite nanoparticles', *Acta Mater.*, 2017, **15**, pp. 416–424
[6] Easo, S.L., Mohanan, P.V.: 'Dextran stabilized iron oxide nanoparticles: synthesis, characterization and in vitro studies', *Carbohydr. Polym.*, 2013, **92**, (1), pp. 726–732
[7] Lu, Y., Yin, Y., Mayers, B.T., *et al.*: 'Modifying the surface properties of superparamagnetic iron oxide nanoparticles through a sol–gel approach', *Nano Lett.*, 2002, **2**, (3), pp. 183–186

[8] Hufschmid, R., Arami, H., Ferguson, R.M., *et al.*: 'Synthesis of phase-pure and monodisperse iron oxide nanoparticles by thermal decomposition', *Nanoscale*, 2015, **7**, (25), pp. 11142–11154

[9] Ge, S., Shi, X., Sun, K., *et al.*: 'Facile hydrothermal synthesis of iron oxide nanoparticles with tunable magnetic properties', *J. Phys. Chem. C*, 2009, **113**, (31), pp. 13593–13599

[10] Jamshidiyan, M., Shirani, A.S., Alahyarizadeh, G.H.: 'Solvothermal synthesis and characterization of magnetic Fe_3O_4 nanoparticle by different sodium salt sources', *Mater. Sci.*, 2017, **35**, pp. 50–57

[11] Solano, E., Perez-Mirabet, L., Martinez-Julian, F., *et al.*: 'Facile and efficient one-pot solvothermal and microwave-assisted synthesis of stable colloidal solutions of MFe2O4 spinel magnetic nanoparticles', *J. Nanopart. Res.*, 2012, **14**, (8), p. 1034

[12] Kataria, N., Garg, V.K.: 'Green synthesis of Fe_3O_4 nanoparticles loaded sawdust carbon for cadmium (II) removal from water: regeneration and mechanism', *Chemosphere*, 2018, **208**, pp. 818–828

[13] Cai, Y., Shen, Y., Xie, A., *et al.*: 'Green synthesis of soya bean sprouts-mediated superparamagnetic Fe_3O_4 nanoparticles', *J. Magn. Magn. Mater.*, 2010, **322**, (19), pp. 2938–2943

[14] Yew, Y.P., Shameli, K., Miyake, M., *et al.*: 'Green synthesis of magnetite (Fe_3O_4) nanoparticles using seaweed (kappaphycus alvarezii) extract', *Nanoscale Res. Lett.*, 2016, **11**, (1), p. 276

[15] Arokiyaraj, S., Saravanan, M., Prakash, N.U., *et al.*: 'Enhanced antibacterial activity of iron oxide magnetic nanoparticles treated with Argemone mexicana L. Leaf extract: an in vitro study', *Mater. Res. Bull.*, 2013, **48**, (9), pp. 3323–3327

[16] Venkateswarlu, S., Kumar, B.N., Prathima, B., *et al.*: 'A novel green synthesis of Fe_3O_4-Ag core shell recyclable nanoparticles using Vitis vinifera stem extract and its enhanced antibacterial performance', *Physica B: Condens. Matter.*, 2015, **457**, pp. 30–35

[17] Park, Y., Hong, Y.N., Weyers, A., *et al.*: 'Polysaccharides and phytochemicals: a natural reservoir for the green synthesis of gold and silver nanoparticles', *IET Nanobiotechnol.*, 2011, **5**, (3), pp. 69–78

[18] Zhang, Z., Li, L., Liu, C., *et al.*: 'Solvothermal synthesis of mesoporous Fe_3O_4 nanoparticles in mixed solvent of ethylene glycol and water: structure and magnetic properties', *J. Supercond. Nov. Magn.*, 2016, **32**, p. 757

[19] Thalapaneni, N.R., Chidambaram, K.A., Ellappan, T., *et al.*: 'Inhibition of carbohydrate digestive enzymes by *Talinum portulacifolium* (forssk) leaf extract', *J. Complement. Integr. Med.*, 2008, **5**, pp. 1553–3840

[20] Babu, R.K., Vinay, K., Sameena, S.K., *et al.*: 'Antihyperglycemic and antioxidant effects of *Talinum portulacifolium* leaf extracts in streptozotocin diabetic rats: A dose-dependent study', *Pharmacogn. Mag.*, 2009, **5**, pp. 1–10

[21] Mohapatra, S., Mallick, S.K., Maiti, T.K., *et al.*: 'Synthesis of highly stable folic acid conjugated magnetite nanoparticles for targeting cancer cells', *Nanotechnology*, 2007, **18**, p. 385102

[22] Kmetz, A.A., Becker, M.D., Lyon, B.A., *et al.*: 'Improved mobility of magnetite nanoparticles at high salinity with polymers and surfactants', *Energy Fuel*, 2016, **30**, pp. 1915–1926

[23] Muxika, A., Etxabide, A., Uranga, J., *et al.*: 'Chitosan as a bioactive polymer: processing, properties and applications', *Int. J. Biol. Macromol.*, 2017, **105**, pp. 1358–1368

[24] Ng, W.L., Yeong, W.Y., Nain, M.W.: 'Polyelectrolyte gelatin-chitosan hydrogel optimized for 3D bioprinting in skin tissue engineering', *Int. J. Bioprinting*, 2016, **2**, pp. 53–62

[25] Xing, K., Zhu, X., Peng, X., *et al.*: 'Chitosan antimicrobial and eliciting properties for pest control in agriculture: a review', *Agron. Sustain. Dev.*, 2015, **35**, pp. 569–588

[26] Senthilkumar, P., Surendran, L., Sudhagar, B., *et al.*: 'Hydrothermal assisted Eichhornia crassipes mediated synthesis of magnetite nanoparticles (E-Fe_3O_4) and its antibiofilm activity', *Mater. Res. Express*, 2019, **6**, p. 095405

[27] Illés, E., Tombácz, E., Szekeres, M., *et al.*: 'Novel carboxylated PEG-coating on magnetite nanoparticles designed for biomedical applications', *J. Magn. Magn. Mater.*, 2015, **380**, pp. 132–139

[28] Arakha, M., Pal, S., Samantarrai, D., *et al.*: 'Antimicrobial activity of iron oxide nanoparticle upon modulation of nanoparticle-bacteria interface', *Sci. Rep.*, 2015, **5**, p. 14813

[29] Parandhaman, T., Pentela, T., Ramalingam, B., *et al.*: 'Metal nanoparticle loaded magnetic-chitosan microsphere: water dispersible and easily separable hybrid metal nano-biomaterial for catalytic applications', *ACS Sustainable Chem. Eng.*, 2016, **5**, pp. 489–501

[30] Ding, Y., Shen, S.Z., Sun, H., *et al.*: 'Design and construction of polymerized-chitosan coated Fe_3O_4 magnetic nanoparticles and its application for hydrophobic drug delivery', *Mater. Sci. Eng. C*, 2015, **48**, pp. 487–498

[31] Vaghari, H., Jafarizadeh-Malmiri, H., Mohammadlou, M., *et al.*: 'Application of magnetic nanoparticles in smart enzyme immobilization', *Biotechnol. Lett.*, 2016, **38**, pp. 223–233

[32] Khalkhali, M., Sadighian, S., Rostamizadeh, K., *et al.*: 'Synthesis and characterization of dextran coated magnetite nanoparticles for diagnostics and therapy', *BioImpacts: BI*, 2015, **5**, p. 141

[33] Senthilkumar, P., Yaswant, G., Kavitha, S., *et al.*: 'Preparation and characterization of hybrid chitosan-silver nanoparticles (chi-Ag NPs); A potential antibacterial agent', *Int. J. Biol. Macromol.*, 2019, **141**, pp. 290–298

[34] Sharma, V.K., Johnson, N., Cizmas, L., *et al.*: 'Review of the influence of treatment strategies on antibiotic resistant bacteria and antibiotic resistance genes', *Chemosphere*, 2016, **1**, pp. 702–714

[35] Blair, J.M., Webber, M.A., Baylay, A.J., *et al.*: 'Molecular mechanisms of antibiotic resistance', *Nat. Rev. Microbiol.*, 2015, **13**, p. 42

[36] Blanco, P., Hernando-Amado, S., Reales-Calderon, J., *et al.*: 'Bacterial multidrug efflux pumps: much more than antibiotic resistance determinants', *Microorganisms.*, 2016, **4**, p. 14

[37] Høiby, N., Bjarnsholt, T., Givskov, M., *et al.*: 'Antibiotic resistance of bacterial biofilms', *Int. J. Antimicrobiol. Agents*, 2010, **35**, pp. 322–332

[38] Fabres-Klein, M.H., Santos, M.J., Klein, R.C., *et al.*: 'An association between milk and slime increases biofilm production by bovine *Staphylococcus aureus*', *BMC Vet. Res.*, 2015, **11**, p. 3

[39] Dufour, D., Leung, V., Lévesque, C.M.: 'Bacterial biofilm: structure, function, and antimicrobial resistance', *Endod. Topics*, 2010, **22**, pp. 2–16

[40] Markovíc, D., Deeks, C., Nunney, T., *et al.*: 'Antibacterial activity of Cu-based nanoparticles synthesized on the cotton fabrics modified with polycarboxylic acids', *Carbohydrates*, 2018, **200**, pp. 173–182

[41] Fereshteh, F., Jebela, S., Almasib, H.: 'Morphological, physical, antimicrobial and release properties of ZnO nanoparticles-loaded bacterial cellulose films', *Carbohydrates*, 2016, **149**, pp. 8–19

[42] Wayane, P.: 'Performance standard for antimicrobial susceptibility testing, clinical and laboratory standards institute (CLSI)'. 26th Informational supplement, Wayne, PA, USA, 2016, vol. **33**, p. M100-S23

[43] Freeman, D.J., Falkiner, F.R., Keane, C.Y.: 'New method for detecting slime production by coagulase negative staphylococci', *J. Clin. Pathol.*, 1989, **42**, pp. 872–874

[44] Nithya, C., Devi, M.G., Karutha Pandian, S.: 'A novel compound from the marine bacterium Bacillus pumilus S6-15 inhibits biofilm formation in gram-positive and gram-negative species', *Biofouling*, 2011, **27**, pp. 519–528

[45] Kouhbanani, M.A.J., Beheshtkhoo, N., Amani, A.M., *et al.*: 'Green synthesis of iron oxide nanoparticles using Artemisia vulgaris leaf extract and their application as a heterogeneous Fenton-like catalyst for the degradation of methyl orange', *Mater. Res. Express*, 2018, **5**, p. 115013

[46] Buazar, F., Baghlani-Nejazd, M.H., Badri, M., *et al.*: 'Facile one-pot phytosynthesis of magnetic nanoparticles using potato extract and their catalytic activity', *Starch-Starke*, 2016, **68**, pp. 796–804

[47] Nehra, P., Chauhan, R.P., Garg, N., *et al.*: 'Antibacterial and antifungal activity of chitosan coated iron oxide nanoparticles', *Br. J. Biomed. Sci.*, 2018, **75**, pp. 13–18

[48] Jayakumar, R., Menon, D., Manzoor, K., *et al.*: 'Biomedical applications of chitin and chitosan-based nanomaterials – A short review', *Carb. Pol.*, 2010, **82**, pp. 227–232

[49] Awwad, A.M., Salem, N.M.: 'A green and facile approach for synthesis of magnetite nanoparticles', *J. Nanosci. Nanotechnol.*, 2016, **2**, pp. 208–213

[50] Elsherbini, A.A., Saber, M., Aggag, M., *et al.*: 'Laser and radiofrequency-induced hyperthermia treatment via gold-coated magnetic nanocomposites', *Int. J. Nanomed.*, 2011, **6**, p. 2155

[51] Inbaraj, B.S., Tsai, T.Y., Chen, B.H.: 'Synthesis, characterization and antibacterial activity of superparamagnetic nanoparticles modified with glycol chitosan', *Sci. Technol. Adv. Mater.*, 2012, **13**, p. 015002

[52] Manikantan, J., Ramalingam, H.B., Shekar, B.C., *et al.*: 'Physical and optical properties of HfO_2 NPs–synthesis and characterization in finding its feasibility in opto-electronic devices', *Adv. Powder. Technol.*, 2017, **28**, pp. 1636–1646

[53] Pati, S.S., Singh, L.H., Guimarães, E.M., *et al.*: 'Magnetic chitosan-functionalized Fe_3O_4@ Au nanoparticles: synthesis and characterization', *J. Alloys Compd.*, 2016, **684**, pp. 68–74

[54] Takai, Z.I., Mustafa, M.K., Asman, S.: 'Preparation of high-performance conductive polyaniline magnetite (PANI/Fe_3O_4) nanocomposites by sol-gel method', *Asian J. Chem.*, 2018, **30**, pp. 2625–2630

[55] Unsoy, G., Yalcin, S., Khodadust, R., *et al.*: 'Synthesis optimization and characterization of chitosan-coated iron oxide nanoparticles produced for biomedical applications', *J. Nanopart. Res.*, 2012, **14**, p. 964

[56] Tokarek, K., Hueso, J.L., Kuśtrowski, P., *et al.*: 'Green synthesis of chitosan-stabilized copper nanoparticles', *Eur. J. Inorg. Chem.*, 2013, **28**, pp. 4940–4947

[57] Jayaseelan, C., Ramkumar, R., Rahuman, A.A., *et al.*: 'Green synthesis of gold nanoparticles using seed aqueous extract of Abelmoschus esculentus and its antifungal activity', *Ind. Crop. Prod.*, 2013, **45**, pp. 423–429

[58] Senthilkumar, P., Kumar, D.R., Sudhagar, B., *et al.*: 'Seagrass-mediated silver nanoparticles synthesis by Enhalus acoroides and its α-glucosidase inhibitory activity from the gulf of mannar', *J. Nanostructure Chem.*, 2016, **6**, pp. 275–280

[59] Nasrollahzadeh, M., Atarod, M., Sajadi, S.M.: 'Green synthesis of the Cu/Fe_3O_4 nanoparticles using Morinda morindoides leaf aqueous extract: a highly efficient magnetically separable catalyst for the reduction of organic dyes in aqueous medium at room temperature', *Appl. Surf. Sci.*, 2016, **364**, pp. 636–644

[60] Sathishkumar, G., Logeshwaran, V., Sarathbabu, S., *et al.*: 'Green synthesis of magnetic Fe_3O_4 nanoparticles using Couroupita guianensis aubl. Fruit extract for their antibacterial and cytotoxicity activities', *Artif. Cell. Nanomed. Biotechnol.*, 2018, **46**, pp. 589–598

[61] Zulfikar, M.A., Afrita, S., Wahyuningrum, D., *et al.*: 'Preparation of Fe_3O_4-chitosan hybrid nano-particles used for humic acid adsorption, environ', *Nanotechnol. Monit. Manage.*, 2016, **6**, pp. 64–75

[62] Tiwari, I., Singh, M., Pandey, C.M., *et al.*: 'Electrochemical genosensor based on graphene oxide modified iron oxide–chitosan hybrid nanocomposite for pathogen detection', *Sensor. Actuators B*, 2015, **206**, pp. 276–283

[63] Banerji, B., Pramanik, S.K., Mandal, S., *et al.*: 'Synthesis, characterization and cytotoxicity study of magnetic (Fe_3O_4) nanoparticles and their drug conjugate', *RSC Adv.*, 2012, **2**, pp. 2493–2497

[64] Berne, B.J., Pecora, R.: '*Dynamic light scattering: with applications to chemistry, biology, and physics*' (Courier Dover Publications, New York, Mineola, 2000)

[65] Gittings, M.R., Saville, D.A.: 'The determination of hydrodynamic size and zeta potential from electrophoretic mobility and light scattering measurements', *Colloids Surf. A*, 1998, **141**, pp. 111–117

[66] Slavin, Y.N., Asnis, J., Häfeli, U.O., *et al.*: 'Metal nanoparticles: understanding the mechanisms behind antibacterial activity', *J. Nanobiotechnol.*, 2017, **15**, p. 65
[67] Auffan, M., Rose, J., Wiesner, M.R., *et al.*: 'Chemical stability of metallic nanoparticles: a parameter controlling their potential cellular toxicity in vitro', *Environ. Pollut.*, 2009, **157**, pp. 1127–1133
[68] Agarwala, M., Choudhury, B., Yadav, R.N.: 'Comparative study of antibiofilm activity of copper oxide and iron oxide nanoparticles against multidrug resistant biofilm forming uropathogens', *Indian J. Microbiol.*, 2014, **54**, pp. 365–368